Al-Azhar University Civil Engineering Research Magazine (CERM)
Vol. (40) No. (4) October, 2018

# EXPERIMENTAL AND NUMERICAL INVESTIGATION ON THE SHEAR FLEXURAL BEHAVIOUR OF NSM FRP STRENGTHENED RC BEAMS

**A.A. Saad[a], A. Khalil[b], H.S. Hadad[c], E.M. Arafa[b]**

[a]*Structural Engineering department, Higher Technological Institute, Egypt*
[b]*Structural Engineering department, Faculty of Engineering, Ain Shams University, Egypt*
[c]*Housing and Building National Research Center, P.O.Box 1770, Giza, Egypt*

**الملخص العربى:**

لقد أصبح التدعيم بدفن الأسياخ البوليمرية بالقرب من السطح الخرسانى من أقوى االتقنيات البديلة لنظام التدعيم باللصق الخارجى. بالمقارنة باللصق الخارجى، يكون عنصر التدعيم أقل تعرضا للعوامل الخارجية، كما تضمن طريقة الدفن تماسك قوى بين عنصر التدعيم و الخرسانة المحيطه به. و لكن على الرغم من تحسن أداء التماسك بشكل كبير فى هذه التقنية، إلا أن انفصال عناصر التدعيم بانهيار الغطاء الخرسانى من أكثر الانهيارات الشائع ملاحظتها للكمرات الخرسانية المدعمة بهذه التقنية، و الذى يبدأ و ينتهى دون الوصول لقيم انفعال عالية فى السيخ البوليمرى. و لذا كرس الباحثون جهودهم لإيجاد طريقة تمنع ذلك النوع من الانهيار. فى ذلك البحث، تم استخدام أسياخ بوليمرية بنهايات مستقيمة و أخرى منحنية، علما بأن الهدف من النهايات المنحنية هو أن تعمل كنظام لربط السيخ بالخرسانة و ذلك لتأخير الانهيار بانفصال الغطاء الخرسانى. كما تم عمل دراسة عددية باستخدام طريقة العناصر المحددة للتحقق من النتائج التى تم الحصول عليها معمليا. و بصفة عامة، كان هناك توافق كبير بين كل من النتائج المعملية و العددية.

**ABSTRACT**

Recently, the near-surface-mounted (NSM) FRP has become an attractive alternative to the externally bonded (EB) technique. Compared with the EB technique, the NSM technique is less exposed to external damage sources and provides a stronger bond between the FRP reinforcement and the surrounding concrete. However, one of the most common failure modes of RC beams strengthened with the NSM technique is debonding by the concrete cover separation (CCS), which initiates and completes at low strain level in the NSM reinforcement. Therefore, researchers were devoted to develop some solutions to delay or prevent this type of failure. In this research, two different bar configurations with straight and bent ends were used. The purpose of the bent end is to delay or prevent the CCS failure. A numerical investigation utilizes the non-linear finite element modeling (FEM) was performed in ANSYS® to validate the experimental results. Overall, the numerical results agreed very well with the corresponding experimental results at all stages of loading.

**KEYWORDS**

Strengthening, NSM, CFRP, Debonding, Concrete cover separation, End Anchorage, Finite element modeling, Fracture energy.

## 1 INTRODUCTION

Recently, strengthening of RC structures with near-surface-mounted (NSM) FRP reinforcement has been witnessed as an effective strengthening technique. The NSM technique involves placing the FRP reinforcement into slits pre-cut into the concrete cover in the tension side of the strengthened element. Compared with the EB FRP, the NSM FRP application offers several advantages, e.g. improved bond capacity, less

installation time, capability of being anchored into adjacent members, and post-strengthening protection [1, 2]. However, the improved bond performance does not exclude the possibility of debonding failure, which occurs in the form of ICID (i.e. intermediate crack induced debonding) or CCS (i.e. concrete cover separation). The CCS failure is much more common than the ICID failure, and usually occurs with a failure plane located at the tension steel level.

To control such a type of failure, CFRP U-wraps were used as an external anchoring system [3, 4]. The transverse anchoring was very effective in increasing the ultimate flexural capacity of tested beams by either delaying the CCS [3] or shifting the failure mode to concrete crushing or CFRP wrap rapture [4]. Sharaky et al. [3, 5-7] investigated the bond and flexural behaviour of RC beams strengthened with NSM FRPs with different material types, epoxy properties, bar sizes, and numbers of NSM bars. To delay CCS failure, mechanical end anchors were applied by drilling vertical holes of 10 mm diameter and 200 mm depth to install steel bars inside them. The steel bars were connected to an assembly, which contained a steel plate with a steel tube welded to it. The FRP element was anchored to the concrete by bonding its end inside the steel tube. The results demonstrated that the mechanical anchoring delayed the CCS failure, and increased the stiffness, yield load, and maximum load capacity.

Besides the extensive experimental work, numerical 3D-FE analyses were also used by many researchers to evaluate the influence of many parameters [8-14]. The perfect bond assumption (no-slip/no-gap) at bar-epoxy and epoxy-concrete interfaces is not capable of predicting the FRP debonding failure, which significantly over-estimates the maximum load and the corresponding deflection [8, 9, 14]. Therefore, accounting the debonding behaviour in the FEM of NSM FRP strengthened beams is necessary to develop an accurate simulation.

In this research, the authors used a new bar configuration with 90° bent ends to delay the CCS failure, in addition to examining the effect of the FRP cross sectional area. On the other hand, a numerical investigation was also carried out using ANSYS® FE analysis program and compared to the experimental results. The developed FE models incorporated bond behaviour at the epoxy-concrete interface. The predicted and experimental results were compared in terms of load-deflection behaviour and failure mode.

## 2 EXPERIMENTAL PROGRAM

### 2.1 Test Specimens

Four RC beams with 150×250 mm rectangular section and 2500 mm total length were constructed and tested to study their flexural-shear behaviour. One beam was tested without strengthening, whereas the other three beams were strengthened with NSM CFRP bars. The tension and compression reinforcements consisted of two 10 mm in diameter deformed steel bars. The shear reinforcement consisted of 8 mm diameter smooth steel stirrups, uniformly spaced at 100 mm. Fig. 1 shows the geometry and reinforcement details of the tested beam.

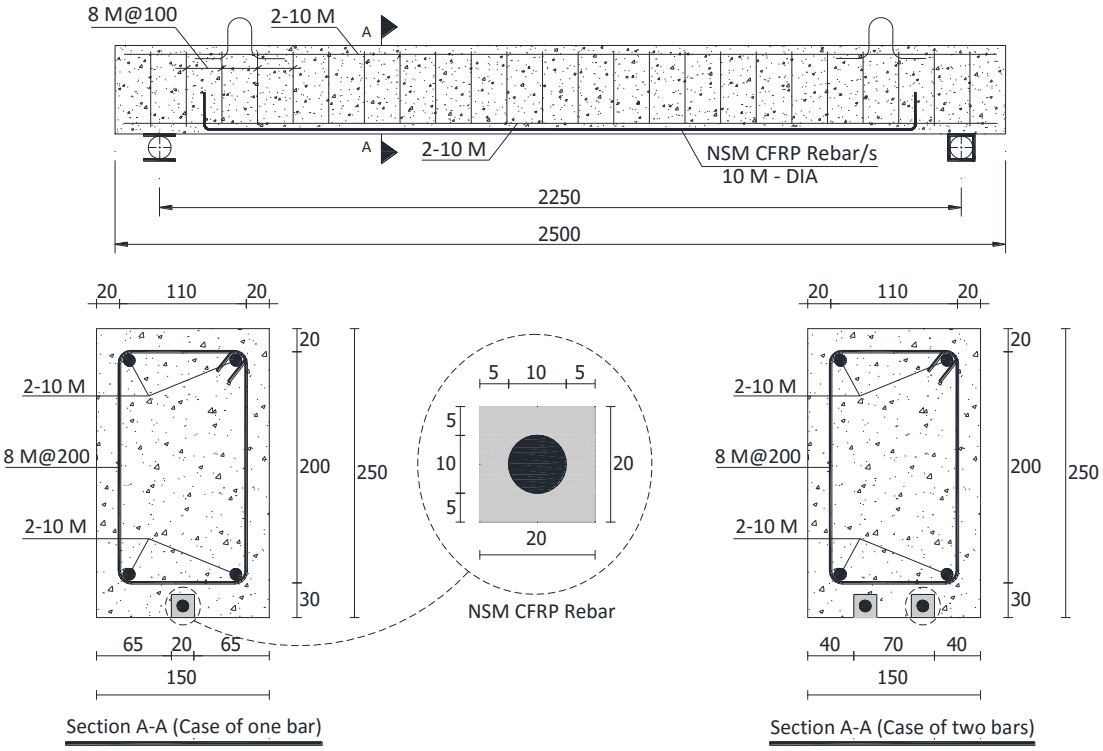


**Fig. 1:** Details of the tested beams

## 2.2 Material Properties

All the tested beams were cast using a ready mixed concrete with a specified 28-days compressive strength of 28 MPa. The concrete compressive strength was determined according to ASTM C39 [15], using six standard concrete cylinders (150×300 mm). The reinforcing steel properties were determined according to ASTM A370 [16]. The yield stress, ultimate strength, and modulus of elasticity were 560 MPa, 630 MPa, and 185 GPa, respectively; while the yield and ultimate tensile strains were 0.0031 and 0.055. An epoxy adhesive, type MBRACE-ADH 4000 (BASF) was used in this study. According to the manufacturer, the tensile strength and modulus of elasticity of the adhesive are 32 and 4300 MPa. The CFRP bars had a deformed surface configuration and a nominal diameter of 10 mm. The tensile strength and modulus of elasticity for the used CFRP bars obtained from the uniaxial tension tests according to ACI 440.3R-12 [17] were 1800 MPa and 130 GPa, respectively.

## 2.3 Specimens and Strengthening Technique

In order to locate the NSM bars, square grooves with a 20 mm side length were pre-formed by placing horizontal and vertical foam inserts inside the casting moulds. Before bonding the NSM bars to the preformed grooves, the internal surfaces of these grooves were carefully roughened and then cleaned by using pressurized air. The two-component epoxy was mixed in a high-speed mixer according to the manufacturer specifications. Each groove was filled with the epoxy paste to cover about 2/3 of its volume. The CFRP bar was gently inserted into the groove and lightly pressed to displace the bonding agent. Extra adhesive was then added to completely fill the groove. The excess epoxy was removed with a spatula, and then the surface was carefully finished. The epoxy adhesive was left to cure at room temperature for one week before testing.

One beam was tested without any strengthening and served as a control beam for comparison purposes. Three beams (S1F, S2F, and A2F) were strengthened with NSM CFRP bars with a limited length of 2000 mm, and two different end conditions (straight and bent). The bent ends were 100 mm height. Beam S1F was strengthened with one straight bar. Beam S2F was strengthened with two straight bars. Beam A2F was strengthened with two bars with bent ends. The purpose of the bent ends is to act as end anchors that might delay the CCS failure.

### 2.4 Test Setup and General Instrumentation

The four beams were tested in three-point bending with a clear flexural span of 2250 mm and a concentrated load at the mid-span up to failure. The load was applied using a 1000 kN capacity servo-controlled hydraulic jack, and monitored using a 500 kN capacity load cell. Three linear variable displacement transducers (LVDT) with 120 mm range were used to measure the deflection at the midspan and underneath the loading points. Strains at the level of the main tension steel and NSM CFRP bar were monitored at the midspan using electrical resistance 120 ohms strain gauges. Moreover, two PI gauges were attached to one of the tested beam sides to measure the concrete compressive and tensile strains.

## 3 RESULTS AND DISCUSSION

Table 1 summarizes the flexural behaviour of the tested beams. The failure mode of each tested beam is indicated in the last column of the table. The effects of the test variables of the flexural response of the tested beam are discussed below. In this table, $P_y$ and $\Delta_y$ are the yielding load and its corresponding deflection, $P_u$ and $\Delta_u$ are the ultimate load and its corresponding deflection, $\Omega$ is the energy absorption which is defined as the area under (P-$\Delta$) curve, and $K_e$ is the effective pre-yield stiffness.

**Table 1:** Key points of load-deflection curves; Comparison of test results with FE results

### 3.1 Failure Modes and Load-Deflection Behaviour

| Beam ID | Results | $P_y$ kN | $\Delta_y$ mm | $P_u$ kN | $\Delta_u$ mm | $K_e$ kN/m | $\Omega$, kN.mm | FM |
|---|---|---|---|---|---|---|---|---|
| CB | Test | 31.9 | 7.9 | 38.5 | 26.6 | 3112.6 | 2373.6 | CC |
| | FE | 29.8 | 7.1 | 38.7 | 22.3 | 3137.3 | 2179 | CC |
| | Error (%) | -6.6 | -10.3 | 0.52 | -16.2 | 0.79 | -8.2 | |
| S1F | Test | 50.3 | 9.7 | 78.8 | 29.3 | 4568.1 | 1905.4 | CCS |
| | FE | 48.2 | 9.2 | 84 | 31.9 | 4636 | 1980 | CCS |
| | Error (%) | -4.2 | - 5.5 | 6.5 | -1.1 | -0.8 | 3.9 | |
| S2F | Test | 72.7 | 10.6 | 102.5 | 20.6 | 6289.8 | 1386.1 | CCS |
| | FE | 69 | 9.75 | 106 | 20.4 | 6201.5 | 1311 | CCS |
| | Error (%) | -5 | -8 | 3.41 | -1.25 | 1.4 | -5.4 | |
| A2F | Test | 70.5 | 10 | 108 | 24.9 | 6502.7 | 1787.3 | CCS |
| | FE | 67.8 | 9.75 | 112 | 23.3 | 6256.5 | 1701 | CCS |
| | Error (%) | - 3.87 | - 2.5 | 3.7 | - 6.6 | -3.7 | - 4.8 | |

Failure modes of the strengthened beams are presented in Fig. 2. The control beam (CB) failed by concrete crushing after yielding of the steel reinforcement, while beams S1F, S2F, and A2F failed by concrete cover separation (CCS). The CCS started in beam S1F by the formation of a flexural shear crack initiated near the constant moment zone, while it started by the formation of a shear crack near the end of the CFRP bar in the two other beams.

The load-midspan deflection (P-Δ) response of the tested beams is shown in Figure 4. Generally, the beams exhibited a semi-tri-linear response defined by three stages. The first stage corresponds to the beam behaviour before cracking. The behaviour in this stage was linear elastic and the NSM reinforcement did not contribute to increase the stiffness. In the second stage, the beam started to crack at the midspan section where the maximum moment was located. Further increase of load, the cracks became wider and new flexural cracks initiated. Many uniformly distributed narrow cracks, with different depths, were observed along the whole length of the tested beam. The developed cracks did not cross the adhesive because of its low elastic modulus. Furthermore, a nonlinear behaviour was observed up to failure. In this stage, the NSM reinforcement significantly increased the stiffness, and decreased the crack widths comparing with the control beam. The second stage ends with yielding of the steel reinforcement. Comparing to the control beam (CB), the yielding load was increased by 57.70% for beam S1F, while it increased by 127.9% and 121.00% for beams S2f and A2F, respectively.

The third stage starts by yielding of the steel reinforcement and ends with the failure of the tested beams. After the steel yielding, the crack width was controlled by the NSM bar. The global stiffness of the tested beams decreased in this stage due to yielding of the steel reinforcement and the weak modulus of the NSM reinforcement. The percentage increase in strength of each beam over the control beam is illustrated in Table 1. As indicated from Table 1, using the NSM CFRP bars significantly increased the ultimate carrying capacity of the strengthened beams compared with the un-strengthened beam. Beam S1F, strengthened with one straight CFRP bar, failed at a load of 78.5 kN; achieving 104.70% increase in the ultimate load over the control beam. As the failure was governed by CCS, doubling the FRP area increased the ultimate load up to 102.50 KN for beam S2F recording 166.25% over that of control beam. The A2F beam, strengthened with two fully bonded end-anchored bars, failed at a load of 108 KN with 180.55% and 5.40% increases over the control and S2F beams, respectively. Therefore, the end hooks were effective in delaying the CCS failure and subsequently increasing the ultimate load.

### 3.2 Cracking Behaviour of the tested beams

Generally, cracking behaviour of the tested beam is divided into two phases: the crack formation phase and stabilized cracking phase. In the first phase, the cracks formed at random locations according to locally weak sections. At each cracked section, the bond action between concrete and steel was lost and the tensile stress in concrete dropped to zero. Away from the crack, the concrete was able to pick up tensile stresses until the bond action was again lost and a new crack started to from at a certain distance. This distance is identified as the crack spacing, which mainly depends on the bond properties (i.e. the better bond between concrete, steel, and NSM reinforcement, the shorter crack spacing). As the strengthened beams were tested with the same tensile steel area, the crack spacing differed from a beam to another according to the bond between concrete and NSM reinforcement.

Doubling the FRP cross sectional area in beam S2F reduced the crack spacing compared to beam S1F; this is because increasing the FRP area decreased the developed tensile force in the CFRP bar, which enhanced the bond between concrete and NSM reinforcement.

**(a)** Beam S1F

**(b)** Beam S2F

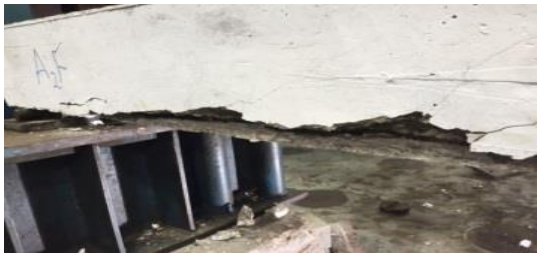

**(c)** Beam A2F

**Fig. 2:** Failure modes of the tested beams

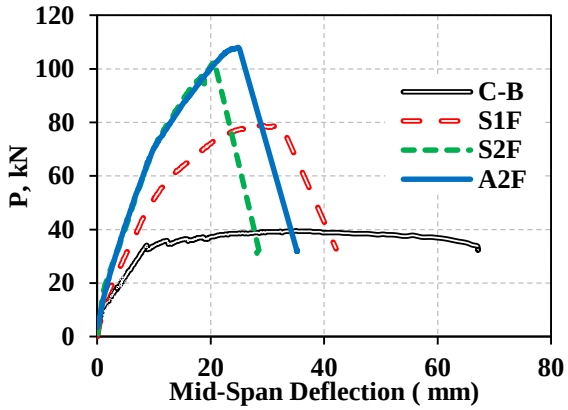


**Fig. 3:** Load-deflection curves for the tested beams

### 3.3 Load-Strain Response at the midspan of the tested beams

In this section, the load-strain (P-ε) response is discussed and compared for the tested beams. The (P-ε) responses in the CFRP bar, tension steel and extreme compression fiber of concrete at the midspan location are shown in Fig. 4.

Generally, up to concrete cracking in tension, the strain increased in a linear manner with the increase of the applied load. After cracking, all the tensile forces carried by concrete were transferred to the tension steel and NSM reinforcement. As a result, the flexural stiffness of the beam decreased causing a reduction in the slope of the (P-ε) curve; however the relation remained linear up to yielding of the tension steel. After yielding, the flexural stiffness of the beam was significantly reduced and another decrease occurred in the slope of the (P-ε) curves.

response was similar to the load-deflection (P-Δ) response. Strengthening with two CFRP bars instead of one bar in beam S2F significantly decreased the developed CFRP strains at the same load compared with beam S1F. Existence of the end anchors in beam A2F reduced the developed CFRP strains compared to beam S2F. The CFRP bars reached 8702 με and 5719 με at the failure of beams S1F and S2F, respectively. Therefore, with respect to beam S1F, doubling the cross sectional area of the CFRP bars reduced the developed FRP strain at failure by 34.3%. Doubling the NSM CFRP shifted the initiation point of the CCS failure. The CFRP bars reached 6611 με at the failure of beam A2F achieving a 15.5% increase over beam S2F.

The measured steel strain at yielding ranged between 2932 με and 3731 με, which is slightly higher than the average yield strain of 3111 με for the tested steel bars. This is possibly due to the tension stiffening effect generated at the bottom of the tested beams. It can be seen in Fig. 4 that doubling the cross sectional area of the CFRP bars in beam S2F significantly decreased the measured steel strains at the same load levels compared to beam S1F.

Strains in the top compression fibers of concrete were calculated based on the linear extension of the recorded strain readings which were measured using the PI-displacement transducers.

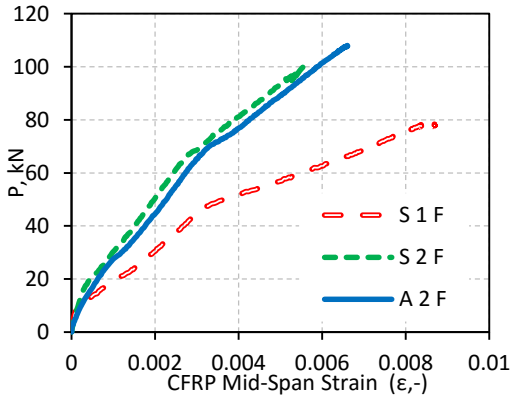


**(a) Load-CFRP strain response**

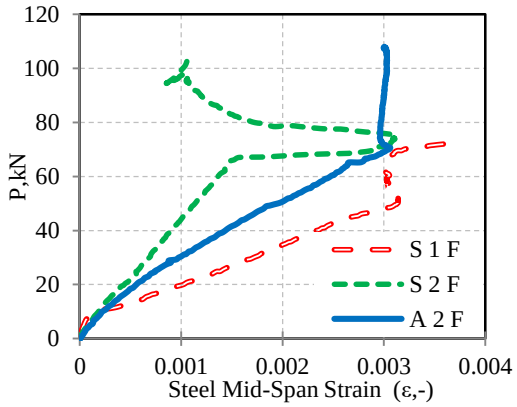


**(b) Load-steel strain response**

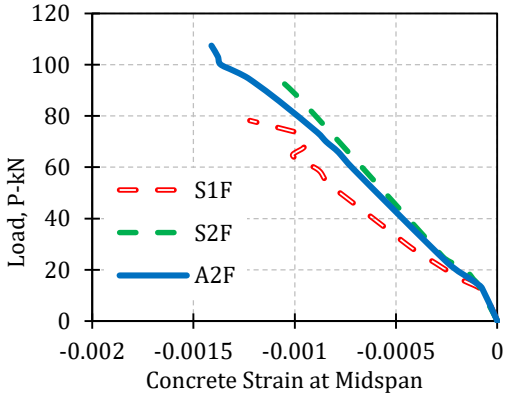


**(c) Load-concrete strain response**

**Fig. 4: Load-midspan strain responses of the tested beams**

## 4 FINITE ELEMENT MODEL

Only one quarter of the RC beam was modelled due to the symmetry of geometry and loading conditions. A double symmetry case was simulated by restraining the displacements in the directions perpendicular to the symmetry planes.

Eight-node solid brick element (SOLID65) was used to model the concrete and epoxy adhesive. The crushing capability of the solid element was removed for concrete to prevent the premature local failure due to stress concentration under loading plates. The steel reinforcement and NSM CFRP bars were modelled using 3D 2-Node structural bar element (LINK180). The perfect bond (No slip occurrence) was considered between the steel reinforcement and concrete as well as between the NSM bar and epoxy. Eight-node solid brick element (SOLID185) was used to model the loading and supporting apparatus. The element is defined by eight nodes having three degrees of freedom at each node, translations in nodal x, y, and z, with the capability of considering nonlinearity and large deformations.

A multi-linear plastic damage model along with the William and Warnke model [18] were employed to define the failure of concrete. The non-linear plastic behavior of concrete under uniaxial compression was obtained from the Hognestad [19] model. The tensile stress-strain response of concrete is shown in Figure 5

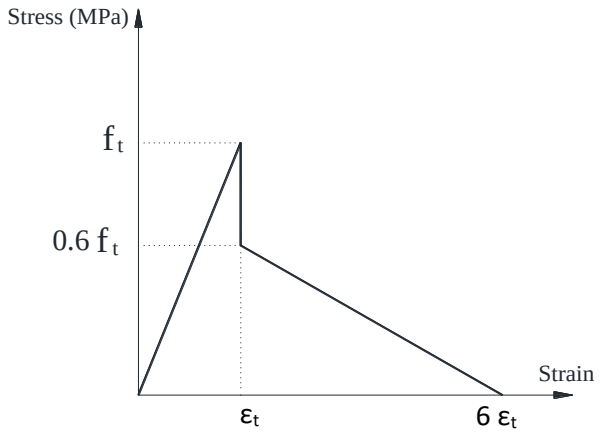


**Fig. 5:** Constitutive model of concrete in tension

The steel reinforcement was assumed to have an elastic-perfectly plastic response with a poison's ratio of 0.30. The Von-Misses failure criterion was used to define yielding of the steel reinforcement. The steel loading and supporting apparatus were modelled as rigid elastic material with a modulus of elasticity and poison's ratio of 200 GPa and 0.30, respectively.

The CFRP material was considered to be linear elastic up to failure. A multi-linear elasto-plastic diagram was used to define the adhesive behaviour along with the same concrete cracking model, but without considering the tension softening phenomenon. A Poison's ratio of 0.35 and 0.37 was assumed for the CFRP and epoxy adhesive, respectively.

### 4.1 Epoxy-Concrete Interaction

Debonding at the epoxy-concrete interface is analyzed by using cohesive zone material (CZM) model and fracture mechanics. Both, contact and interface elements, with zero and finite thickness, respectively, can use the CZM traction-separation constitutive

model in ANSYS®. The contact elements were used for the FE models of the non-anchored NSM systems (in S1F and S2F beams), while the interface elements were used for the FE models of the anchored NSM systems (in the A2F beam).

A mixed-mode bilinear CZM model, predefined in ANSYS®, was used to simulate the interface debonding. In such a model, the interface separation occurs under a combination of three traction modes (mode I: opening, mode II: shear, and mode III: tearing); therefore, this type of debonding is controlled by both shear-slip ($\Gamma$-$\delta$) and tension-gap ($\sigma$-$u$) behaviours. The bilinear shear-slip and tension-gap behaviours are presented in Fig.6.

The ultimate tensile stress ($\sigma_{max}$) and tensile fracture energy ($G_{cn}$) were limited to the tensile strength ($f_t$) and fracture energy of concrete ($G_{ft}$). The tensile fracture energy of concrete was using Eq. 1, which is proposed by CEB-FIP model code [20]. The contact gap at completion of debonding ($u_f$) was obtained using Eq. 2, which was derived by equating the tensile fracture energy of the interface with the tensile fracture energy of concrete. To obtain the maximum interfacial shear stress ($\Gamma_{max}$), Eq. 3 which was proposed by Hassan and Rizkalla [21] was used. An extensive parametric study was conducted to determine the contact slip at completion of debonding ($\delta_f$). The value of $\delta_f$ was taken as 0.35 and 0.25 for beams strengthened with one and two CFRP bars, respectively. The separations values ($u_u$ and $\delta_u$) were assumed to be one quarter of the failure separation values ($u_f$ and $\delta_f$) [12].

$$G_{ft} = (0.0469\, Da^2 - 0.5\, Da + 26)\left(\frac{f'c}{10}\right)^{0.70} \quad \text{Eq. 1}$$

$$u_f = \frac{f_c'^{0.2}}{1.40}(0.0469\, D_a^2 - 0.5\, D_a + 26) \quad \text{Eq. 2}$$

$$\Gamma_{max\ (epoxy\text{-}concrete)} = \frac{ft\,\mu}{1.40} \quad \text{Eq. 3}$$

, where $D_a$ is the maximum aggregate size and $\mu$ is the epoxy-concrete friction coefficient; a value of $\mu = 1$ was used [2].

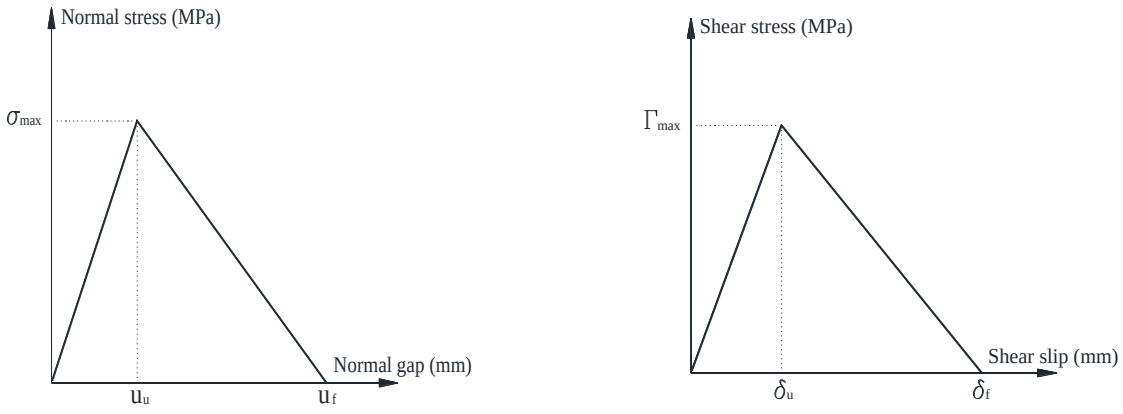


**(a) Normal-gap model** **(b) Shear-slip model**

**Fig. 6: Bilinear Normal-gap and shear-slip models**

## 4.2 Non-Linear Analysis

The non-linear solution was operated using a force control mode with a 10 N load increment. In contrast with the displacement control mode, the force control mode consumes a little time in solving such complex models; however, it cannot track the post-peak behaviour of the modelled specimen.

The FE models were developed with refined mesh applied at the locally high stressed zones. Fig. 7 shows the used mesh in the developed models.

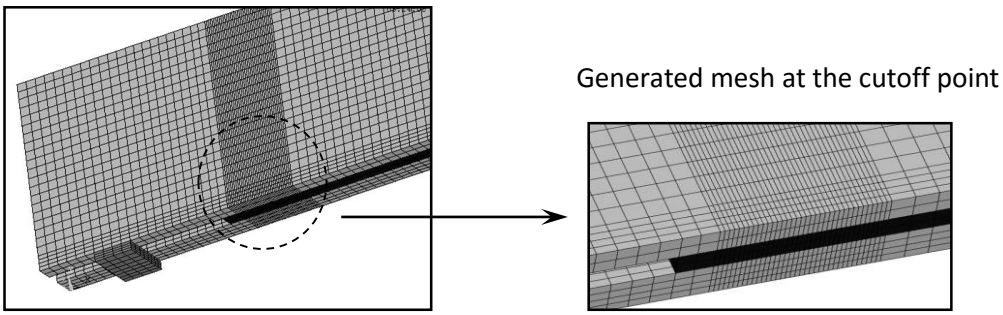


**Fig. 7: Mesh of the developed FE models**

Failure of the developed FE models was defined according to two mechanisms: (a) crushing of the concrete after yielding of the steel reinforcement and (b) concrete cover separation. The modelled specimen is considered to be failed by concrete crushing if the compressive strain reaches the value of 0.003. The concrete cover separation was detected by the examination of the equivalent plastic strain of concrete at the level of the failure plane which was experimentally observed. The modelled RC beam was assumed to fail by CCS when the effective plastic tensile strain at the level of the tension steel exceeds the rapture strain of concrete.

## 4.3 Finite Element Results

### *4.3.1 Validation of the FE results*

Fig. 8 shows a comparison between the experimental and numerical load-deflection curves for all the tested RC beams. At yielding stage, the differences between the experimental and FE values are negligible. However, the obtained ultimate loads from the FE models are slightly higher than those obtained from the experimental records. This in fact is due to ignoring the radial stresses transferred from the tension steel and NSM bars to the concrete in the developed FE models. The comparison details are enlisted in Table 1.

The comparison indicates that there is a good correlation between the developed models and the recorded experimental results at all stages of loading up to failure.

The FE load-CFRP strain response at the midspan was compared to that obtained from the experimental results in Fig. 9. Generally, the slight differences between the analytical and experimental results can be related to the CFRP modulus, which is not absolutely constant and could be slightly smaller or greater than the specified value.

Based on the compared load-deflection behaviour, load-CFRP strain response, and failure modes, both validity of the developed FE models and reliability of the FE simulation are confirmed.

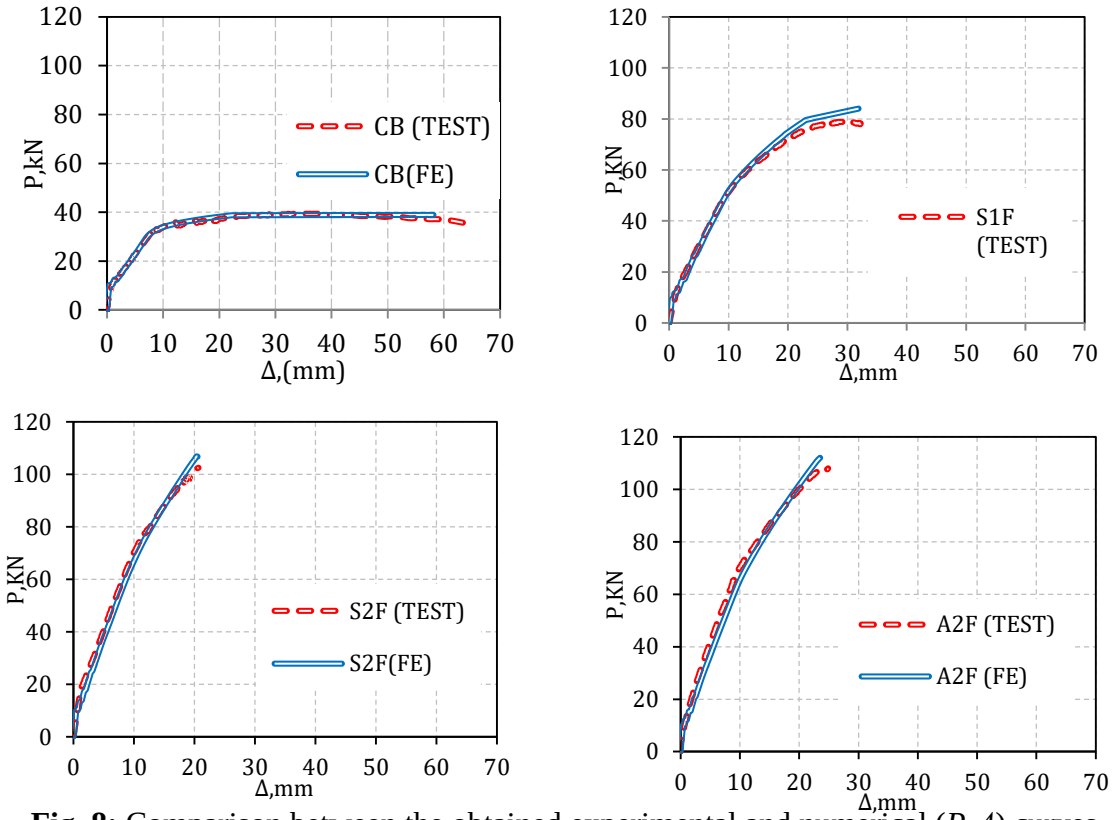


**Fig. 8:** Comparison between the obtained experimental and numerical (*P-Δ*) curves

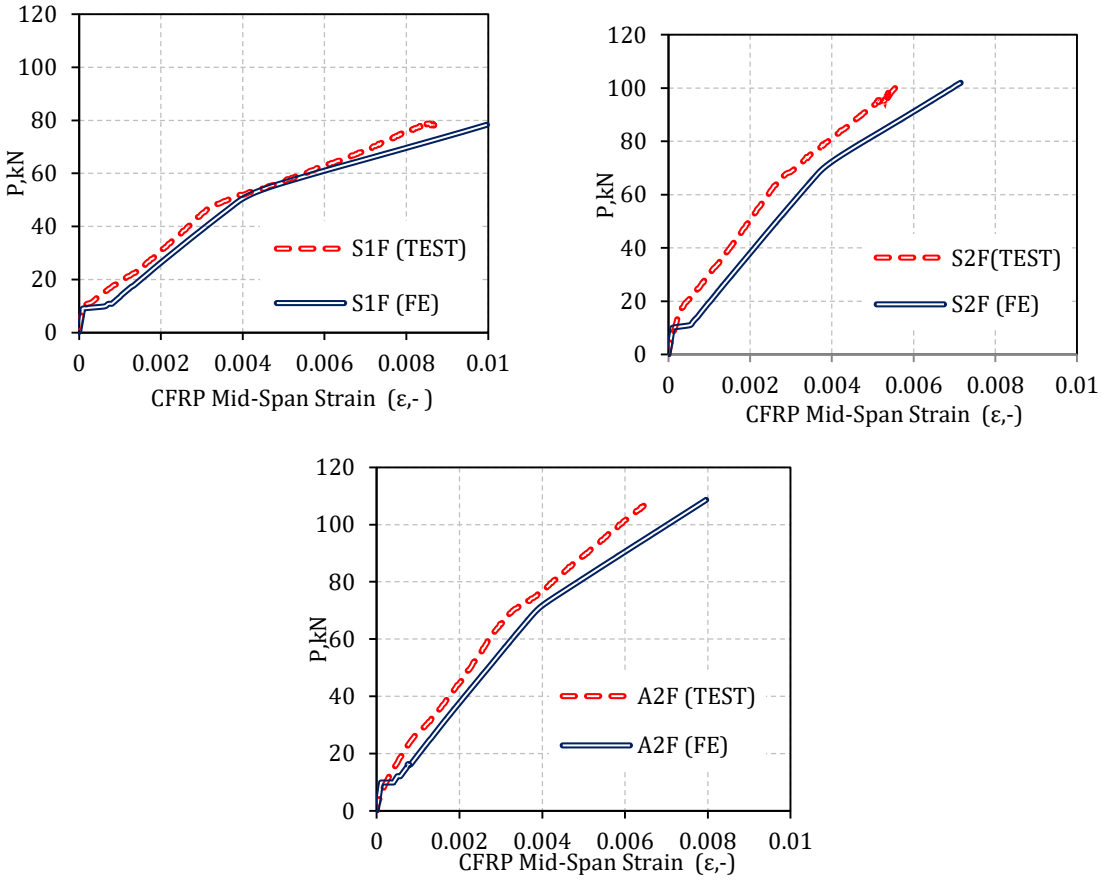


**Fig. 9:** Comparison between the experimental and numerical load-CFRP strain curves

## 5 CONCLUSIONS

Based on the obtained experimental and numerical results, the following main conclusions can be drawn:

1- Strengthening with the NSM CFRP bars is very effective in increasing both flexural strength and stiffness. The NSM strengthening system improved the load-deflection response of the tested beams, and limited the deflections and crack widths at different loading stages. The concrete cover separation was the predominant failure mode of all the strengthened beams.

2- It is noticeable that doubling the FRP cross area produce a great significant increase in the ultimate carrying capacity and stiffness scoring 29.6% and 37.7% respectively, over the beam strengthened by one straight bar.

3- Strengthening with the end-anchored CFRP bars delayed the CCS failure and increased the ultimate load compared with the straight CFRP bars.

4- The developed FE models properly simulated the flexural behaviour of RC beams strengthened with NSM anchored and non-anchored CFRP bars. The strain-based failure criteria used to predict the CCS failure mode was able to simulate the cracking behaviour of the developed FE models.

Original practical recommendations are provided in this paper including:

1- Anchoring the NSM bars to delay the concrete cover separation failure;

2- Considering the mixed mode debonding in the FE analysis to improve the accuracy;

3- Examining the equivalent plastic strain gradient to detect the concrete cover separation failure in the FE programs.

## 6 REFERENCES

[1] Parretti, R. and A. Nanni, Strengthening of RC members using near-surface mounted FRP composites: Design overview. Advances in Structural Engineering, 2004. 7(6): p. 469-483.

[2] De Lorenzis, L. and J. Teng, Near-surface mounted FRP reinforcement: An emerging technique for strengthening structures. Composites Part B: Engineering, 2007. 38(2): p. 119-143.

[3] Sharaky, I.A., L. Torres, and H. Sallam, Experimental and analytical investigation into the flexural performance of RC beams with partially and fully bonded NSM FRP bars/strips. Composite structures, 2015. 122: p. 113-126.

[4] Rasheed, H.A., R.R. Harrison, R.J. Peterman, and T. Alkhrdaji, Ductile strengthening using externally bonded and near surface mounted composite systems. Composite Structures, 2010. 92(10): p. 2379-2390.

[5] Sharaky, I.A., L. Torres, J. Comas, and C. Barris, Flexural response of reinforced concrete (RC) beams strengthened with near surface mounted (NSM) fibre reinforced polymer (FRP) bars. Composite Structures, 2014. 109: p. 8-22.

[6] Sharaky, I.A., L. Torres, M. Baena, and C. Miàs, An experimental study of different factors affecting the bond of NSM FRP bars in concrete. Composite Structures, 2013. 99: p. 350-365.

[7] Sharaky, I.A., L. Torres, M. Baena, and I. Vilanova, Effect of different material and construction details on the bond behaviour of NSM FRP bars in concrete. Construction and Building Materials, 2013. 38: p. 890-902.

[8] Kang, J., Y. Park, J. Park, Y. You, and W. Jung. Analytical evaluation of RC beams strengthened with near surface mounted CFRP laminates. 7th International Symposium: Fiber-Reinforced Polymer (FRP) Reinforcement for Concrete Structures. 2005.

[9] Omran, H. and R. El-Hacha. Finite element modelling of RC beams strengthened in flexure with prestressed near surface mounted CFRP rebars. Proceeding of the 8th international conference on short and medium span bridge (SMSB 2010). August. 2010.

[10] Soliman, S.M., E. El-Salakawy, and B. Benmokrane, Flexural behaviour of concrete beams strengthened with near surface mounted fibre reinforced polymer bars. Canadian Journal of Civil Engineering, 2010. 37(10): p. 1371-1382.

[11] Omran, H.Y. and R. El-Hacha, Nonlinear 3D finite element modeling of RC beams strengthened with prestressed NSM-CFRP strips. Construction and Building Materials, 2012. 31: p. 74-85.

[12] Hawileh, R.A., Nonlinear finite element modeling of RC beams strengthened with NSM FRP rods. Construction and Building Materials, 2012. 27(1): p. 461-471.

[13] Rezazadeh, M., S. Cholostiakow, R. Kotynia, and J. Barros, Exploring new NSM reinforcements for the flexural strengthening of RC beams: Experimental and numerical research. Composite Structures, 2016. 141: p. 132-145.

[14] Sharaky, I., R. Reda, M. Ghanem, M. Seleem, and H. Sallam, Experimental and numerical study of RC beams strengthened with bottom and side NSM GFRP bars having different end conditions. Construction and Building Materials, 2017. 149: p. 882-903.

[15] ASTM. Standard test method for compressive strength of cylindrical concrete specimens. ASTM C39/C39M. American Society for Testing and Materials, West Conshohocken, PA, USA; 2010.

[16] ASTM. tandard test methods and definitions for mechanical testing of steel produces. ASTM A370. American Society for Testing and Materials, Pennsylvania, USA; 2010.

[17] ACI 440.3R-12. Guide for test methods for fiber reinforced polymers (FRP) for reinforcing and strengthening concrete structures. In: ACI Committee 440, American Concrete Institute, Farmington Hills, Mich.; 2012.

[18] Willam, K.J. and E. Warnke, Constitutive model for the triaxial behavior of concrete. International association of bridge and structural engineers, Seminar on concrete structure subjected to triaxial stresses, paper III-1, Bergamo, Italy, May 1974. IABSE Proc. 19, 1975.

[19] Hognestad, E., N.W. Hanson, and D. McHenry. Concrete stress distribution in ultimate strength design. Journal Proceedings. 1955.

[20] FIB Bulletin 10. Bond of reinforcement in concrete. Tech. Rep; 2000.

[21] Hassan, T. and S. Rizkalla, Bond mechanism of NSM FRP bars for flexural strengthening of concrete structures. ACI Structural Journal, 2004. 101(6): p. 830-839.